ARRIVAL TIME CONTROLLABILITY OF A CONSTRAINED TAILORED ARRIVAL PATH AND ITS OPTIMIZATION

Noboru TAKEICHI*, Daigo INAMI*, Masahiro KUDO, and Naoki FUJII****
***Nagoya University, Japan, ****Electronic Navigation Research Institute, Japan**

Keywords: *Tailored Arrival, Flight Path, RNAV, Air Traffic Control*

Abstract

The arrival time controllability of tailored arrival (TA) paths and its optimization are discussed. A TA path is designed using the least number of track-to-fix and the radius-to-fix legs neglecting the engine thrust. They are numerically analyzed so as to satisfy a set of appropriate boundary conditions both at the top of descent (TOD) and landing considering practical aircraft conditions, such as flap settings and flight envelope. The arrival time controllability is defined as the differences between the fastest and the slowest arrival time. Through several series of the arrival time analyses, it is found that the TA paths determined by changing the way-point positions can achieve the larger arrival time controllability than those determined by changing the TOD position. The feasibility of the TA path optimization from the viewpoint of the traffic controllability is also presented. It is shown to be possible to compose an arrival path with the maximum arrival time controllability without any additional fuel consumption.

1 Introduction

The continuous descent approach[1] (CDA) has been strongly focused and examined in detail because the aircraft approach noise and the fuel consumption are both drastically reduced[2]. The tailored arrival (TA) is proposed to facilitate CDA even in a congested airspace[3]. In TA operation each aircraft is provided with a specifically designed flight path from the air traffic controller that simultaneously facilitates the separation and the CDA. The TA path is indicated through the fixed waypoints (WPs) and the time to pass them, and the aircraft change the top of descent (TOD) position and the flight path angle to satisfy the indicated arrival time[4]. When a larger or smaller arrival time control is required, the addition or omission of WPs is also necessary to stretch or reduce the flight path length[4,5] in addition to the adjustment of the TOD position. It must also be noticed that the TA path with larger flight path angle for the faster arrival time requires the longer cruise distance, which results in the larger fuel consumption.

Modern aircraft is able to fly on an arbitrary flight path quite accurately owing to the advanced flight management system and the precise area navigation (RNAV) systems such as the GPS augmentation systems[6]. It is expected that future navigation systems will make it possible to indicate the TA path through arbitrarily determinable WPs unlike the current TA paths. Concerning the RNAV aided arrival paths, some studies have been carried out for the aircraft noise mitigation[7,8]. The authors have focused on its arrival time controllability. Through numerical investigations using a quite simplified aircraft model, the TA path optimization from the view point of the traffic controllability is demonstrated, and the TA path with the maximum arrival time controllability is presented[9].

In this paper, some series of numerical analyses are carried out using a practical aircraft model, which includes actual flap settings and actual flight envelope. Two types of the TA paths are considered; one is determined through the arbitrarily determinable WPs and fixed TOD, and the other is through the fixed WPs as the current ones. Hereafter, the former path is called

Fixed TOD Path, and the latter one is called Fixed WP Path. The standard CDA path is also defined so that the aircraft descent from the TOD and enter the final glide path through one turning leg. The arrival time analysis is carried out by comparing the arrival time between the TA paths and the standard CDA path. The arrival time controllability is defined as the achievable time difference of TA paths, and its optimization is demonstrated. The arrival paths are designed according to the standard for the RNP approach[10] so that general aircraft are able to fly along it with only small deviations.

2 Flight Path Composition

The arrival paths are composed of Radius to Fix legs (RF legs) and the Track to Fix legs (TF legs)[10]. In the standard, an RF leg and a TF leg are defined as a constant radius circular path about a defined turn center that terminates at a fix and a geodesic path between two fixes. The standard CDA paths are defined so that the aircraft begins descent from the TOD without changing its cruise flight direction, and enter the final glide path through only one turning leg as shown in Fig. 1a. In this figure, the TF legs and RF leg are denoted as single and double lines, respectively. It is possible to define a family of the standard CDA paths by changing the final glide path length. The TA paths for the arrival time control are designed by adding the least number of flight legs to the standard CDA path.
The Fixed TOD Path is obtained by adding one RF leg and one TF leg and adjusting the final glide path length. The outline of this path is depicted in Fig. 1a. The standard CDA path and the Fixed TOD Path are denoted as solid and dashed lines, respectively. Both faster and slower arrival paths are obtained by adjusting the final glide path (TF3 leg) length. The Fixed WP Path is designed by adjusting the TOD position as shown in Fig. 1b. This arrangement corresponds to the omission of the RF1 leg of the Fixed TOD Path, and the arrival time control is made through the cruise length and the flight path angles of the TF1 and TF2 legs.

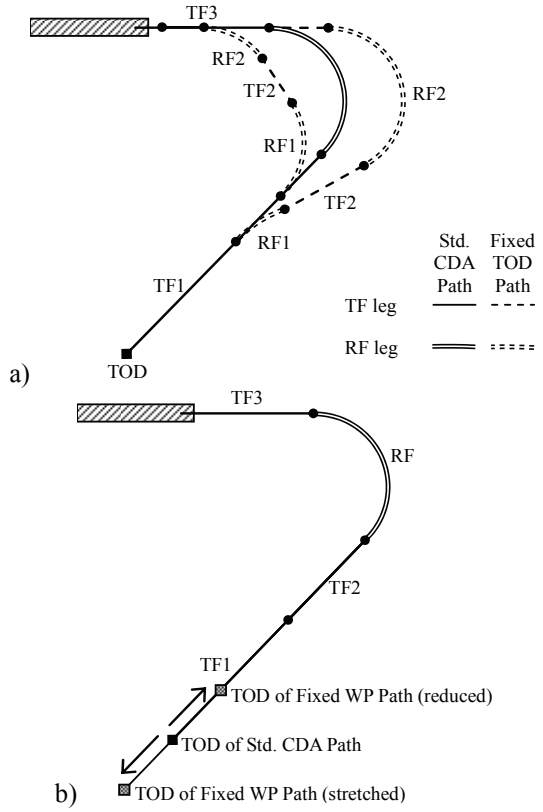

Fig. 1 Outline of Arrival Paths, a: Standard CDA Path and Fixed TOD Path, b: Fixed WP Path[9]

3 Equations of Motion and Boundary Conditions

The TA paths are analyzed so that the aircraft values of state in the equations of motion (1) ~(6) satisfy the boundary conditions at the TOD and the end of TF3 leg. For the clarity of the problem, the engine thrust in idle state is assumed to be negligibly small. The TOD position x_{TOD} and y_{TOD} are obtained through the standard CDA path analyses using the boundary conditions Eq. (7) at the TOD and Eq. (9) at the end of TF3 leg. The same boundary conditions Eqs. (7) and (9) are used in the Fixed WP Path analyses. In the Fixed TOD Path analyses, the same TOD as the standard CDA path given in Eq. (8) is used for the TOD boundary condition.
The TA paths are numerically obtained using the parameters of B777-300[11]. The altitude and the velocity are 11278m (37000ft) and 250m/s (486kt) at the TOD, and 305m (1000ft) and 80m/s (156kt) at the end of TF3 leg. Three stage flap settings are made; cruise, approach, and landing configurations. Table 1 summarizes the

conditions to determine these configurations. The maximum and minimum operating speed, $v_{\max}$ and $v_{\min}$ in calibrated air speed (CAS), are also considered in the numerical analyses. The aircraft parameters are shown in Table 2. The standard bank angle in RF leg is given as 18deg[10].

The numerical analyses to solve the boundary value problem and the optimization have been carried by using MATLAB Optimization Toolbox [12]. The dimensionless form of the equations are applied[13], where the time, length, and mass of the state variables are transformed dimensionless by v^*/g , v^{*2}/g , and $\rho^* S v^{*2} C_L^*/2g$, respectively, where the variables with superscript * are the cruise state values.

$$m\frac{dv}{dt} = -\frac{1}{2}\rho S\left(C_{D0} + C_{Di}C_L^2\right)v^2 - mg\sin\gamma \quad (1)$$

$$mv\frac{d\gamma}{dt} = \frac{1}{2}\rho S C_L v^2\cos\sigma - mg\cos\gamma \quad (2)$$

$$mv\frac{d\psi}{dt} = \frac{1}{2}\rho S C_L v^2\frac{\sin\sigma}{\cos\gamma} \quad (3)$$

$$\frac{dh}{dt} = v\sin\gamma \quad (4)$$

Table 1 Aircraft Cinfigurations[11]

Cruise	$h \ge h_{\max,AP}$ or $h < h_{\max,AP}$ and $v_{CAS} \ge v_{\min,CR} + 10kt_{CAS}$
Approach	$h_{\max,AP} > h \ge h_{\max,LD}$ and $v_{CAS} < v_{\min,CR} + 10kt_{CAS}$ or $h < h_{\max,LD}$ and $v_{CAS} \ge v_{\min,AP} + 10kt_{CAS}$
Landing	$h < h_{\max,LD}$ and $v_{CAS} < v_{\min,AP} + 10kt_{CAS}$

(note: $h_{\max,AP} = 8000\,ft$,and $h_{\max,LD} = 3000\,ft$)

Table 2 Aircraft Parameters[11]

m [kg]	2.38×10^5	C_{D0} (Cruise)	1.69×10^{-2}
S [m^2]	4.28×10^2	C_{Di} (Cruise)	4.89×10^{-2}
$v_{\max}$ [kt$_{CAS}$]	3.30×10^2	C_{D0} (Approach)	2.25×10^{-2}
$v_{\min,CR}$ [kt$_{CAS}$]	2.08×10^2	C_{Di} (Approach)	4.96×10^{-2}
$v_{\min,AP}$ [kt$_{CAS}$]	1.57×10^2	C_{D0} (Landing)	8.69×10^{-2}
$v_{\min,LD}$ [kt$_{CAS}$]	1.44×10^2	C_{Di} (Landing)	4.68×10^{-2}

$$\frac{dx}{dt} = v\cos\gamma\cos\psi \quad (5)$$

$$\frac{dy}{dt} = v\cos\gamma\sin\psi \quad (6)$$

$$h_{ini} = h^* = 11277.6m(=37000\,ft),\quad \psi_{ini} = \psi^*,\quad v_{ini} = v^* = 250m/s \quad (7)$$

$$h_{ini} = h^* = 11277.6m(=37000\,ft),\quad \psi_{ini} = \psi^*,\quad v_{ini} = v^* = 250m/s,\quad x_{ini} = x_{TOD},\quad y_{ini} = y_{TOD} \quad (8)$$

$$h_{fin} = 304.8m(=1000\,ft),\quad v_{fin} = 80m/s,\quad \psi_{fin} = 0rad,\quad x_{fin} = 0m,\quad y_{fin} = 0m \quad (9)$$

4 Arrival Time Analyses

4.1 Standard CDA Path

The standard CDA path is analyzed using the -3 deg flight path angle in both the final glide path and RF leg. It is assumed that the aircraft arrives from the 90 deg azimuth angle from the runway in this paper. A series of the standard CDA paths are obtained by changing the final glide path length as shown in Fig. 2, where z axis is 10 times magnified. The origin of the x and y axes coincide with the end of the final glide path. The joints of the legs are denoted as circles, and the ground projection of the flight path is shown as the thin lines. In this chapter, the standard CDA path with 25km final glide path length is focused as an example, and the arrival time difference from this standard path is analyzed. This path is indicated by * in Fig. 2. The flight path angle of TF1 leg is -2.76deg, and the standard arrival time is 1241.4sec. Fig. 3 shows

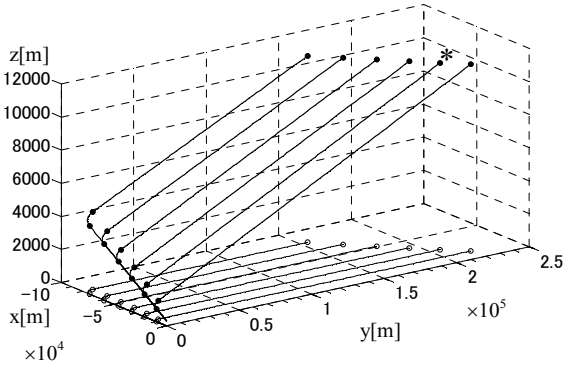

Fig. 2 Standard CDA Paths

the time-histories of the true air speed (TAS), CAS, azimuth angle, and altitude of this standard CDA path.

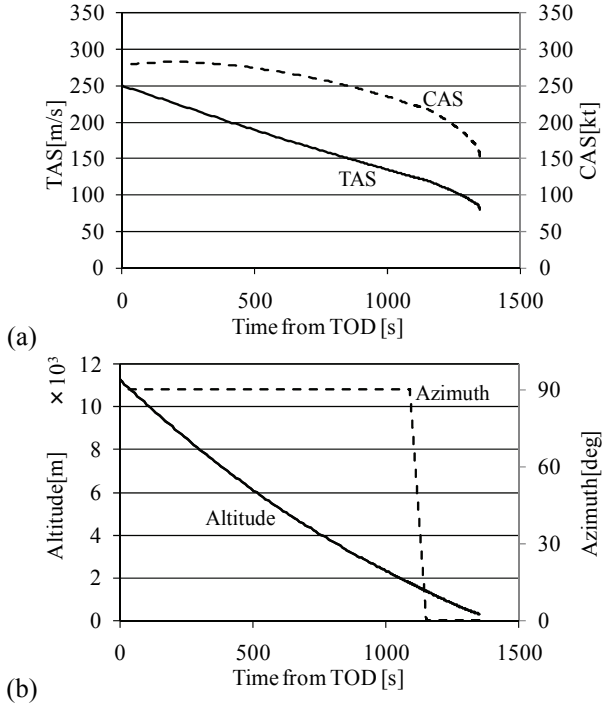

Fig. 3 Time-History of Standard CDA Path, a: TAS and CAS, b: Altitude and Azimuth

4.2 Arrival Time Difference Behavior of Fixed TOD Paths

4.2.1 Flight Path Angle

The arrival time behavior and controllability of the Fixed TOD Paths is analyzed in this section. The Fixed TOD Paths are numerically obtained so that they satisfy the same boundary conditions as the standard CDA paths. In the arrival time analyses, the flight path angles shown in Table 2 are applied. The RF2 and TF3 leg correspond to the final approach segment, and the flight path angle is fixed to be -3 deg.

Table 2 Flight Path Angle used in Path Analyses

TF1	RF1	TF2	RF2	TF3
γ_1	γ_2	γ_2	-3deg	-3deg

4.2.2 Faster Arrival Path

Faster arrival paths are obtained by shortening the TF3 leg. By determining the RF2 leg turning angle $\Delta\psi_{RF2}$ and the TF3 leg flight time t_{TF3}, a faster arrival path satisfying the boundary conditions is solely obtained. Such a path determination corresponds to the indication of the initial and final points of each leg as the WPs.

The fastest arrival path is obtained when $t_{TF3} = 0\,\text{sec}$, where the roll out point of the RF2 leg coincides to the point of the final boundary conditions. In this case, $\Delta\psi_{RF2} = 61.2\,\text{deg}$, $\gamma_1 = -3.21\,\text{deg}$ and $\gamma_2 = -2.06\,\text{deg}$, are obtained from the numerical analysis. The shape of this path is depicted in Fig. 4 denoted by diamonds (♦), where x and z axis are 5 and 10 times magnified. The time-histories of TAS, CAS, azimuth angle, and altitude are summarized in Fig. 5. The maximum CAS becomes equal to $v_{\max}$ in the TF1 leg. This result means that the fastest path is determined by the final glide path length limit ($t_{TF3} = 0\,\text{sec}$) and the CAS limit,

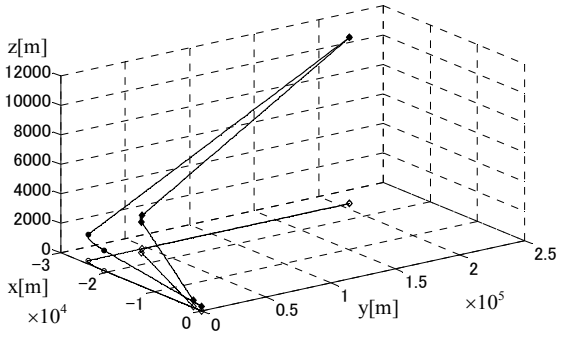

Fig. 4 Arrival Path Shape, ♦:Fastest, ●:Standard

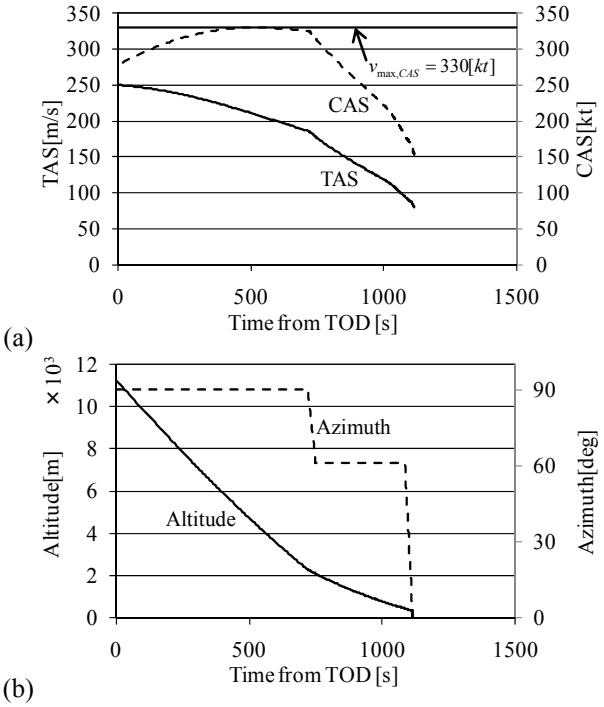

Fig. 5 Time-History of Fastest Fixed TOD Path, a: TAS and CAS, b: Altitude and Azimuth

and a possible combination of the $\Delta\psi_{RF2}$ and γ_2 is solely determined to satisfy the boundary conditions. Its arrival time difference from the standard CDA path is $\Delta t_{fin}^{\min} = -236.5\,\text{sec}$.

4.2.3 Slower Arrival Path

It is also possible to obtain slower arrival paths by extending the TF3 leg. In the same way as the faster arrival paths, a slower arrival path satisfying the boundary conditions is solely determined for a longer final glide path.

The slowest arrival path is obtained when the final glide path length is 23.8km ($t_{TF3} = 225.9\,\text{sec}$) and $\Delta\psi_{RF2} = 91.4\,\text{deg}$. In this case, the flight path angles are $\gamma_1 = -2.07\,\text{deg}$ and $\gamma_2 = -2.94\,\text{deg}$, and the arrival time difference from the standard path is $\Delta t_{fin}^{\max} = 123.3\,\text{sec}$. Figures 6 and 7 shows the path shape and the time-histories of TAS, CAS, azimuth angle, and altitude.

4.3 Arrival Time Difference Behavior of Fixed WP Paths

The Fixed WP Paths are obtained by moving the TOD in the arrival direction as shown in Fig. 1b. Slower arrival path is obtained by shortening the cruise length and applying the smaller flight path angle. The faster arrival path is obtained by extending the cruise length and applying the larger flight path angle. The Fixed WP Paths are analyzed by finding a combination of γ_1 and γ_2 to satisfy the boundary conditions.

The fastest and slowest paths are shown in Fig. 8 denoted as ♦ and +, respectively. Figure 9 shows the time-histories of TAS, CAS, azimuth angle, and altitude. In the fastest arrival path, $\gamma_1 = -3.21\,\text{deg}$, $\gamma_2 = -0.05\,\text{deg}$, and the maximum CAS in TF1 leg is equal to $v_{\max}$. The fastest path is determined by the limitation of the CAS in the same way as the fastest Fixed TOD Path. The flight path angles in the slowest path are $\gamma_1 = -2.50\,\text{deg}$ and $\gamma_2 = -2.90\,\text{deg}$. The cruise lengths of the fastest and slowest paths are 18.6km longer and 2.50km shorter than that of the standard CDA path, respectively. The cruise time difference should also be considered in the arrival time analyses using the following equation:

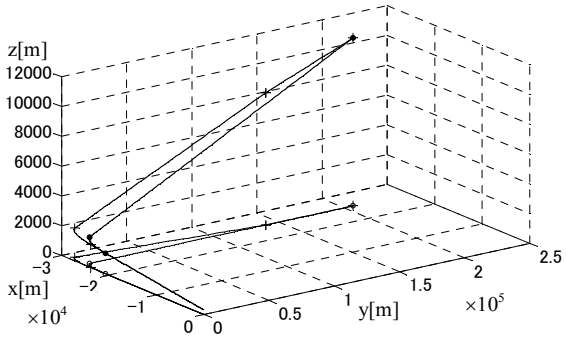

Fig. 6 Arrival Path Shape, +:Slowest, ●:Standard

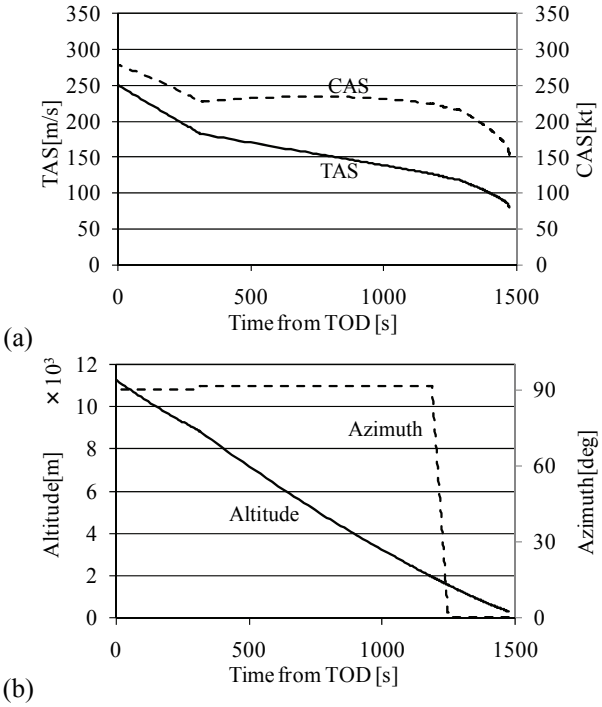

Fig. 7 Time-History of Slowest Fixed TOD Path, a: TAS and CAS, b: Altitude and Azimuth

$$\Delta t_{fin} = \Delta t_{fin}^{TOD} - \frac{\Delta TOD[m]}{v_{ini}[m/s]} = \Delta t_{fin}^{TOD} - \frac{\Delta TOD[m]}{250[m/s]} \quad (10)$$

, where Δt_{fin}^{TOD} is the arrival time measured from the TOD of this path. The arrival time differences obtained from the Eq.(10) were $\Delta t_{fin}^{\min} = -153.4\,\text{sec}$ for the fastest arrival path, and $\Delta t_{fin}^{\max} = 59.9\,\text{sec}$ for the slowest arrival path. In addition, it must be noticed that the amount of the fuel also changes due to the cruise length change. Especially this result in the additional fuel consumption in faster arrival paths. The fuel consumption rate of the B777 aircraft is 117.5kg/min for the cruise at the altitude 37000ft[11], which is equal to 7.83kg/km. In this case, the fastest path requires 146kg fuel in addition to the standard CDA path or the Fixed

TOD Path. On the other hand, the slowest path can achieve almost the same arrival time delay as the Fixed TOD Path with diminishing the fuel consumption about 20kg.

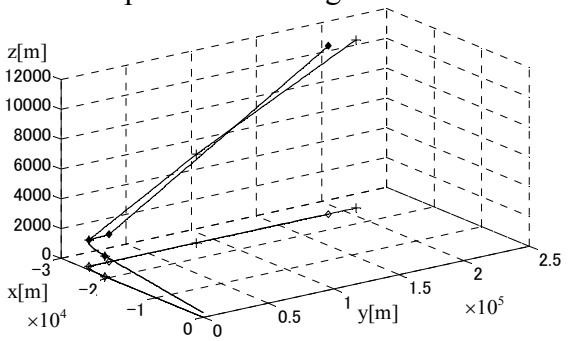

Fig. 8 Fixed WP Path, ♦: Fastest, +: Slowest

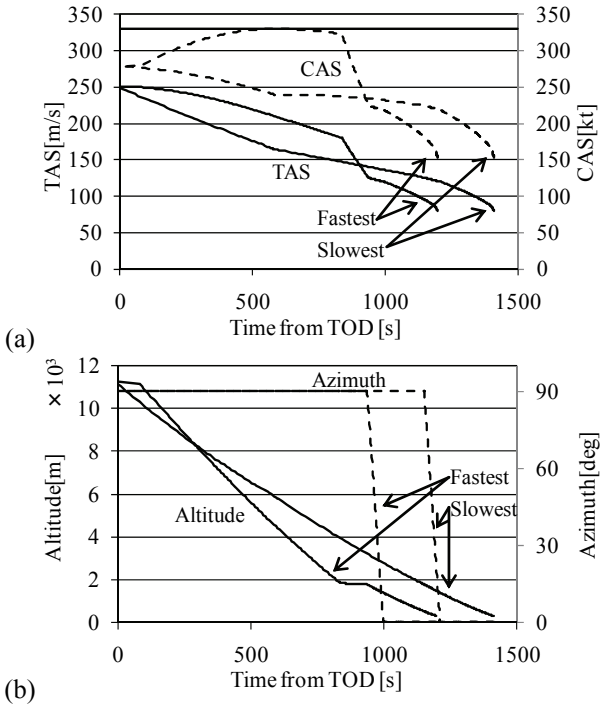

Fig. 9 Time-History of Fixed WP Path,
a: TAS and CAS, b: Altitude and Azimuth

5 Arrival Time Controllability

It is possible to define the arrival time controllability as the difference between the fastest arrival time $\Delta t_{fin}^{\min}$ and the slowest one $\Delta t_{fin}^{\max}$. The maximum arrival time differences $\Delta t_{fin}^{\min}$ and $\Delta t_{fin}^{\max}$, and the controllability $\Delta t_{fin}^{\max} - \Delta t_{fin}^{\min}$ are summarized in Fig. 10. In this case, the arrival time difference and the controllability of the standard CDA paths with the final glide path length of 9.5~84.4km ($t_{TF3} = 100 \sim 600\,\mathrm{sec}$) are analyzed. The vertical axes denote the arrival time difference from the standard CDA paths in Fig. 10a, and the arrival time controllability in Fig. 10b. In Fig. 10a, the lines A and B denote the slowest and fastest arrival time differences of the Fixed TOD Paths, and the lines C and D denote those of the Fixed WP Paths, respectively. The lines E and F in Fig. 10b denote the arrival time controllability of the Fixed TOD Path and the Fixed WP Path.

It is found that the arrival time difference of the fastest Fixed TOD Path (denoted by line B) becomes larger as the longer final glide path is applied. On the contrary, the arrival time difference of the fastest Fixed WP Path (denoted by line D) becomes smaller. Both of the Fixed TOD and Fixed WP fastest arrival paths are obtained when the maximum CAS coincide with the limit values. Both in the Fixed WP and Fixed TOD paths, the aircraft rapidly descents on the TF1 leg with $\gamma_1 = -3.21\,\mathrm{deg}$ to experience the maximum CAS. The TF1 leg length decreases as the final glide path length increases. The faster arrival time difference of the Fixed WP Path also decreases because the arrival time control is made mainly by the Flight path angle of the TF1 leg. On the other hand, the faster arrival time difference of the Fixed TOD Path increases because the path length difference between the standard and the fastest path length becomes larger. However the path length difference turns to decrease as the final glide path length further increases, and the increase rate of the faster arrival time difference becomes smaller as shown in Fig. 10 line B.

Both of the arrival time difference of the slowest Fixed TOD (line A) and Fixed WP (line C) paths decrease in almost the same manner. Because the arrival time of the standard CDA path with longer final glide path becomes larger while the slowest arrival time hardly differ, the difference between the slowest arrival time and the standard one monotonously decreases as shown in Fig. 10 Line A and C.

Because the faster arrival time difference increases with its rate decreasing, and the slower arrival time difference monotonously decreases in the case of the Fixed TOD Paths, the arrival time controllability has a maximum value as shown in line E. The maximum

controllability is realized when $t_{TF3} \approx 300\,\text{sec}$. The difference between the fastest and slowest arrival time is 370.2 sec in this case. Therefore, by defining the flight path with the arrival time difference of $\Delta t_{fin} = -75.7\,\text{sec}$ as the standard arrival one, the maximum controllability of $\pm 185.1\,\text{sec}$ is achieved. Figure 11 shows several arrival paths with the RF2 leg turning angle from 20deg to 80deg ($\Delta\psi_{RF2} = 20 \sim 80\,\text{deg}$), where x and z axis are 5 and 10 times magnified. It is possible to compose a series of

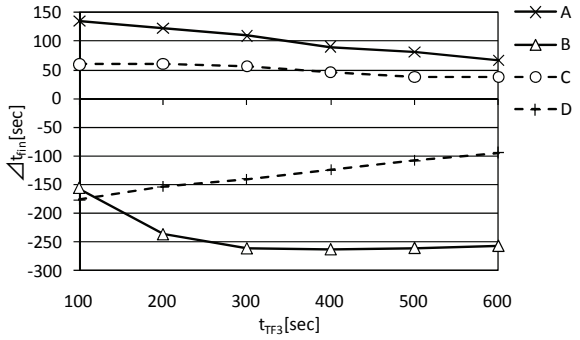

a)

A: Slowest Fixed TOD Path, B: Slowest Fixed TOD Path, C: Slowest Fixed WP Path, D: Slowest Fixed WP Path

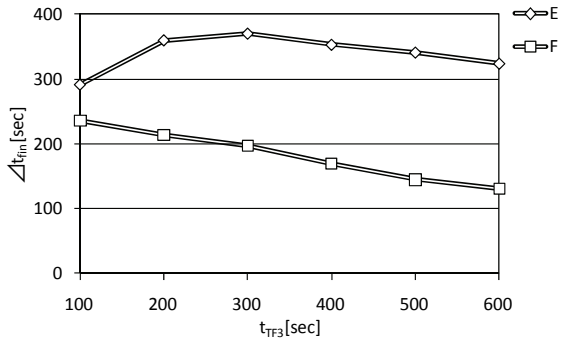

b)

E: Arrival Time Controllability of Fixed TOD Path, F: Arrival Time Controllability of Fixed WP Path

Fig. 10 Arrival Time Difference and Controllability, a: Fastest and Slowest Arrival Time Differences, b: Arrival Time Controllability

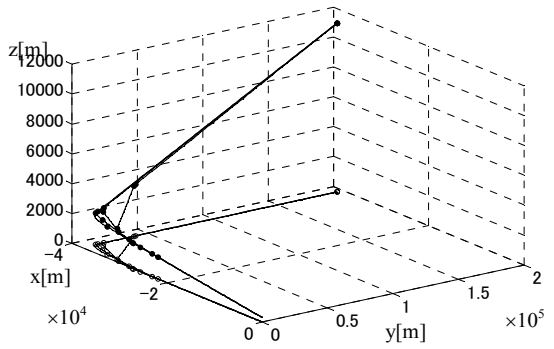

Fig. 11 Arrival Paths with Maximum Arrival Time Controllability

the arrival path with the maximum controllability by determining the combinations of the path parameters t_{TF3} and $\Delta\psi_{RF2}$.

6 Conclusion

The arrival time behavior and its controllability of two types of the tailored arrival paths have been discussed in this paper. It has been clarified that the Fixed TOD Paths can achieve the larger controllability than the Fixed WP Paths. The series of numerical analyses has shown the feasibility to optimize the traffic controllability, and the concept of the arrival path with the maximum controllability is proposed. This TA path can moderate the required accuracy and range of the TOD required time of arrival. It is also shown that the combination of the faster Fixed TOD Path and the slower Fixed WP Path can simultaneously achieve the quasi-optimum arrival time controllability and fuel consumption reduction.

In this paper the arrival time controllability determined by the flight path composition with the least number of flight legs has been discussed through numerical analyses using only one type of aircraft parameter. Therefore, to show the feasibility and practical usefulness of the presented concept, more detailed analyses considering various aircraft types and conditions, and actual flight procedures such as boundary conditions at TOD and landing, aircraft arrival azimuth angle etc. are indispensable in future works. In addition, the effects of many causes of the flight path deviation, such as the aircraft parameters, the navigational and the flight technical errors, the atmospheric conditions, etc, must also be investigated. It is also expected that the further larger arrival time controllability will be achieved by using a larger number of flight legs.

7 References

[1] Clarke, J-P.B., Ho, N.T., Ren, L., Brown, J.A., Elmer, K.R., Tong, K.-O., and Wat, J.K., "Continuous Descent Approach: Design and Flight Test for Louisville International Airport," Journal of Aircraft, Vol. 41, No. 5, 2004, pp. 1054-1066.

[2] Erkelens, L.J.J., "Research on noise abatement procedures," NLR-TP-98066, NLR, Feb. 1998.

[3] Coppenbarger, R.A., Mead, R.W., and Sweet, D.N., "Field Evaluation of the Tailored Arrivals Concept for Datalink-Enabled Continuous Descent Approach," AIAA2007-7778, 7th AIAA Aviation Technology, Integration and Operations Conference (ATIO) 18 - 20 September 2007, Belfast, Northern Ireland.

[4] Coppenbarger. R., Lanier, R., Sweet, D., and Dorsky, S., "Design and Development of the En-Route Descent Advisor for Conflict Free Arrival Metering," AIAA-2004-4875, Proceedings of the AIAA Guidance, Navigation and Control Conference, Providence, RI, Aug. 2004.

[5] Ren, L., and Clarke, J.P.B., "Flight-Test Evaluation of the Tool for Analysis of Separation and Throughput," Journal of Aircraft, Vol. 45, No. 1, Jan.-Feb. 2008, pp. 323-332.

[6] Grewal, M.S., Weill, L.R., and Andrews, A.P., "Global Positioning Systems, Inertial Navigation, and Integration," John Wiley & Sons, New Jersey, United States, 2007, pp. 199-254.

[7] Prats, X, Nejjari, F, Puig, V, Quevedo, J., and Mora-Camino, F., "A Framework for RNAV Trajectory Generation Minimizing Noise Nuisances," Proceedings of the 2nd International Congress on Research in Air Transportation (ICRAT), Belgrade, Serbia, 2006.

[8] Prats, X., Quevedo, J., and Puig, V., "Trajectory Management for Aircraft Noise Mitigation Towards Future ATM/CNS," ENRI International Workshop on ATM/CNS, Tokyo, Japan, Mar. 5-6, 2009.

[9] Takeichi, N., and Inami, D., "Arrival Time Controllability of Tailored Arrival subjected to Flight Path Constraints," Journal of Aircraft, in press.

[10] FAA, "United States Standard for Required Navigation Performance Approach Procedures with Special Aircraft and Aircrew Authorization Required (RNP-SAAAR)," Order 8260.52, Jun. 5, 2005, available online, http://www.airweb.faa.gov/

[11] Eurocontrol Experimental Centre, "User Manual for the Base of Aircraft Data (BADA) Revision 3.7," EEC Technical/Scientific Report No.2009-003, Mar. 2009. (http://www.eurocontrol.int/eec/public/standard_page/proj_BADA.html)

[12] The MathWorks, http://www.mathworks.com/

[13] Tsuchiya, T., "Near-Optimal Guidance Method for Maximizing the Reachable Domain of Gliding Aircraft," Transactions of the Japan Society for Aeronautical and Space Sciences, Vol. 49, No. 165, pp. 137–145, 2006.

Copyright Statement